Glioblastoma models driven by different mutations converge to the proneural subtype

Francesco Alessandrini, Davide Ceresa, Irene Appolloni, Francesca Pagani, Pietro Luigi Poliani, Daniela Marubbi, Paolo Malatesta

PII: S0304-3835(19)30565-8

DOI: https://doi.org/10.1016/j.canlet.2019.11.010

Reference: CAN 114563

To appear in: *Cancer Letters*

Received Date: 18 July 2019

Revised Date: 29 October 2019

Accepted Date: 7 November 2019

Please cite this article as: F. Alessandrini, D. Ceresa, I. Appolloni, F. Pagani, P.L. Poliani, D. Marubbi, P. Malatesta, Glioblastoma models driven by different mutations converge to the proneural subtype, *Cancer Letters*, https://doi.org/10.1016/j.canlet.2019.11.010.

Abstract

The need of reliable syngeneic animal models for gliomas has been addressed in the last decades by reproducing genetic alterations typical of human glioblastoma in the mouse. Since different alterations underlie different molecular glioblastoma subtypes it is commonly expected that tumors induced by specific alterations represent models of the corresponding subtypes. We tested this assumption by a multilevel analysis ranging from a detailed histopathological analysis to a genome-wide expression profiling by microarray and RNA-seq on gliomas induced by two distinct molecular alterations: the overstimulation of the PDGF- and the EGF- pathways. These alterations are landmarks of proneural and classical glioblastoma subtypes respectively. However, our results consistently showed a strong similarity between the two glioma models. The expression profiles of both models converged toward a signature typical of oligodendrocyte progenitor cells, regardless the wide differentiative potential of the cell of origin. A classification based on similarity with human gliomas profiles revealed that both models belong to the proneural subtype.

Our results highlight that reproducing a molecular alteration specific of a glioblastoma subtype not necessarily generates a tumor model recapitulating such subtype.

Glioblastoma models driven by different mutations converge to the proneural subtype

Francesco Alessandrini[a,1], Davide Ceresa[b], Irene Appolloni[b], Francesca Pagani[c], Pietro Luigi Poliani[c], Daniela Marubbi[a,b] and Paolo Malatesta[a,b]

[a]Ospedale Policlinico San Martino – IRCCS, Genoa, Italy.

[b]Department of Experimental Medicine, University of Genoa, Genoa, Italy.

[c]Department of molecular and translational medicine, Pathology Unit, University of Brescia, Brescia, Italy

[1]Present address: Northwestern University - Feinberg School of Medicine, Department of Neurology, 303 Est Chicago Avenue, Chicago, Illinois 60611

Corresponding author: Paolo Malatesta Ospedale Policlinico S. Martino, Largo Rosanna Benzi 10, 16132 Genova, Italy, phone:+390105558403, fax +390105558405, email:paolo.malatesta@unige.it

Running title: PDGF-B and EGFRvIII induced similar murine gliomas

Abstract

The need of reliable syngeneic animal models for gliomas has been addressed in the last decades by reproducing genetic alterations typical of human glioblastoma in the mouse. Since different alterations underlie different molecular glioblastoma subtypes it is commonly expected that tumors induced by specific alterations represent models of the corresponding subtypes. We tested this assumption by a multilevel analysis ranging from a detailed histopathological analysis to a genome-wide expression profiling by microarray and RNA-seq on gliomas induced by two distinct molecular alterations: the overstimulation of the PDGF- and the EGF- pathways. These alterations are landmarks of proneural and classical glioblastoma subtypes respectively. However, our results consistently showed a strong similarity between the two glioma models. The expression profiles of both models converged toward a signature typical of oligodendrocyte progenitor cells, regardless the wide differentiative potential of the cell of origin. A classification based on similarity with human gliomas profiles revealed that both models belong to the proneural subtype.

Our results highlight that reproducing a molecular alteration specific of a glioblastoma subtype not necessarily generates a tumor model recapitulating such subtype.

Keywords: oligodendroglial precursor cells, RTK, mouse model, PDGF-B, EGFRvIII

Abbreviations used:

EGFR, epidermal growth factor receptor

PDGF, platelet-derived growth factor

DsRed, red fluorescent protein isolated from Discosoma

OPC, Oligodendrocyte progenitor cells

PCA, principal component analysis

1. Introduction

In recent years, high-throughput molecular studies by genome wide profiling has allowed a more accurate knowledge of high-grade glioma biology. Classifications of human gliomas in subtypes based on their gene expression profile have been suggested by several authors [1, 2]. Gene expression profiling revealed that glioma cells resemble specific lineages of nervous system: for example, proneural subtype shows oligodendrocyte progenitor cells (OPCs) signature, while classical subtype shows astrocytic signature [2]. However, these resemblances do not necessarily reflect the tumor cell of origin. A correlation is rather established between gene expression profiles and mutations: EGFR gene mutations are prevalent in the classical glioma subtype, NF1 gene mutations in the mesenchymal subtype and PDGFR-A and IDH1 alterations in the proneural subtype.

The different subtypes underlie different biological features and, possibly, a specific response to different therapeutic approaches [3-6], representing to date a major challenge in modeling experimental gliomas. Several murine high-grade glioma models have been developed based on driver mutations found in human patients, according to the hypothesis that genetic aberrations responsible for gliomagenesis play an important role in tumor maintenance too [7]. The importance of molecular alteration over the cell of origin is strongly suggested by observations on PDGF-B induced murine gliomas. These tumors show features typical of human proneural subclass, regardless the multi-lineage differentiation potential of the transduced cells. In particular, PDGF-B transduction of both post-natal, lineage-restricted, progenitor cells [8, 9] and multipotent embryonic radial glial cells [10] generates gliomas constituted by similar oligodendrocyte progenitor–like cells. Given the prominence of the genetic alteration in the definition of tumor subtype, it could be expected that tumor models recapitulating different glioma subtypes may be induced by introducing mutations typical of such subtype in embryonic neural progenitor cells (NPC).

To test this hypothesis, in the present study we thoroughly compared murine high grade gliomas (mHGGs) induced by the alteration of PDGF pathway, typical of the proneural subtype, with those induced by sustained activation of the EGFR, typical of the classical subtype [2, 11]. Both tumor models were generated from orthotopically transplanted embryonic NPC harboring specific genetic lesions: the overexpression of PDGF-B or the expression of the constitutive active EGFR receptor EGFRvIII together with the INK4a/Arf homozygous deletion ($INK4a^{-/-}$; [12].

2. Material and methods

2.1. Animal Procedures

Mice were handled in agreement with the guidelines conforming to current Italian regulations for the protection of animals used for scientific purposes (D.lgs 26/2014) that implements EU Directive 2010/63/EU for animal experimentations. Procedures were approved by the Ethical Committee for Animal Experimentation of the Ospedale Policlinico San Martino and by the Italian Ministry of Health. The experiments were performed with the BALB/c mouse strain, both wild-type and p16/p19 knock-out ($INK4a^{-/-}$).

Mice were anesthetized with a cocktail containing Fentanyl/Midazolam/Metadominine (0.05/5/0.5 mg/kg, respectively), a 5mm scalp incision was performed to expose the bregma area. Up to 2 µl of suspension, containing transduced cells, were injected by a Hamilton syringe guided by a stereotaxic apparatus at bregma coordinates: anterior-posterior, 1.0 mm; lateral, 1.5 mm left and 2.5 mm below the skull surface. After surgery skin was sutured with adsorbable wire (Johnson & Johnson Ethicon Sutures Vicryl 4/0) and mice were awaken by a specific antidote cocktail containing Atipamezol, Flumacenil and Naloxone (2.5/0.5/1.2 mg/kg, respectively). Mice were monitored daily after transplant and killed at first signs of neurological distress or at experiment endpoint. Mice brains were explanted and pictures were taken under a Leica fluorescence stereomicroscope (Wetzlar, Germany).

2.2. Cell cultures and retroviral transduction

Primary murine high grade gliomas expressing DsRed fluorescent reporter were obtained as follows: NPC were dissociated from the whole telencephalon of mouse embryos 14 days post coitum (embryonic day 14; E14) mouse embryos as previously described [13]. NPC were plated at density of $3x10^5$ cells/cm^2 on 24-well plates coated with Matrigel matrix (1:200; BD Biosciences, Franklin Lakes, NJ) and cultured in DMEM-F12 added with B27 supplement, human bFGF and EGF (10 ng/ml). Immediately after plating, cells were transduced with pCAG:DsRed-EGFRvIII or pCAG:DsRed-PDGF retroviral vectors already described [14, 15]. After 7 days $2x10^4$ transduced cells were inoculated intracranially in adult BALB/c mice. Glioma cells were dissociated from explanted tumor masses as previously reported [16] and cells were maintained in the culture medium described above. For the analysis of $INK4a^{-/-}$ NPC population composition, $5x10^5$ acutely

dissociated NPC were plated onto 13mm-diameter coverslips coated with poly-D-lysine, fixed in 4% PFA after 2 hours and immunostained. For the analysis of INK4a$^{-/-}$ NPC differentiative potential and clonal analysis, 2.5x10^5 untransduced NPC, cultured for 5 days in the same conditions as for the cells to be intracranially transplanted, were detached and plated onto 13mm-diameter coverslips coated with poly-D-lysine and incubated in SATO medium [17] for 7 days , then fixed in 4% PFA. For clonal analysis, cells were incubated, immediately after plating, with a low titer viral preparation in order to transduce about 50 cells per coverslip. Clones were then identified basing on the spatial clustering of their members as visualized by the EGFP reporter gene expression.

2.3. Neuropathological analysis and immunostainings

Brains were removed and fixed in 10% formalin. 2-4µm thick paraffin-embedded tissue sections were used for hematoxylin and eosin (H&E) staining and blindly analyzed. For IHC, sections were deparaffinized, rehydrated and endogenous peroxidase activity blocked with in methanol 0.3% H_2O_2 for 20 minutes. Antigen retrieval (when necessary) was performed in either 1.0 mM EDTA buffer (pH 8.0) or 1 mM Citrate buffer (pH 6.0). Sections were then washed in TBS (pH 7.4) and incubated with primary antibodies (see Table 1 in Supplementary Methods) in TBS 1% bovine serum albumin. Reaction was revealed by Novolink Polymer (Leica Microsystems) or Dako EnVision+Dual Link System Peroxidase (Dako Cytomation) detection systems followed by DAB and counterstaining with Hematoxylin. Images were acquired through an Olympus DP70 camera mounted on an Olympus Bx60 microscope using CellF imaging software (Soft Imaging System GmbH). Statistical analyses on quantifications of positive cells were performed with two-sided t-test and are reported as mean ± standard deviation.

For immunofluorescence staining, brains were fixed in 4% paraformaldehyde, cryoprotected in 20% sucrose and sectioned with a Leica CM3050 S cryostat. Sections were washed in PBS and incubated with primary antibodies in PBS with 10% goat serum as described in Table 2 of the Supplementary Methods.. Binding of primary antibody was revealed with fluorescent secondary antibodies as detailed in Supplementary Methods Table 3.

The images of whole coronal brain sections were acquired by epifluorescence microscope (Axio Imager. M2, Zeiss, Oberkochen, Germany) by Slide Explorer2 plug-in of Micromanager [53].

Quantification of percentage of cells in immunostaining analysis has been done by analyzing a minimum of 450 cells per single experiment. Statistical analysis was performed with Student T-test and with a number of

independent samples (nExp) equal or greater than 5, sufficient to reach a power >90% with significant threshold alpha=0.05 on effect size d=2.5.

2.4. Microarray and RNA sequencing analyses

RNA extracted from cells cultured in vitro for less than 10 passages and derived from 2 $_{mHGG}$PDGF and 4 $_{mHGG}$EGFRvIII primary tumors derived from 4 independent NPC cultures were hybridized on Affymetrix GeneChip Mouse Genome 430 2.0 Array (GEO Accession Number GSE133095) by AROS Applied Biotechnology (Aarhus,Denmark). Raw data from transcriptome database for murine astrocytes, neurons, and oligodendrocytes (GSE9566; [18]) and from data of wide gene expression profile of cells from sub ventricular zone (SVZ, GSE58260; [19]) murine adult olfactory bulb stem cells (OBSCs; GSE37516; [20]) and radial glial cells (RG; GSE8034; [21]) performed on the same microarray platform were obtained from literature as CEL format and analyzed with the same procedures of our samples.

Data were analyzed using the R3.4.2 software and BioConductor version 3.5.35 [22]. Expression values were extracted from raw data files using the RMA method built in the affy 1.54.0 library package.. In order to eliminate batch effects, the entire dataset was eventually quantile normalized [23]. Principal component analysis (PCA) and heatmap representations are based on the 1% of the genes showing the highest variance in expression levels between neural lineages. Differentially expressed genes were ranked by using RankProd 3.2.0 library, with PFP=0.05 as threshold for significance.

For RNA sequencing, cells obtained by dissociation of 3 different $_{mHGG}$PDGF and 3 $_{mHGG}$EGFRvIII primary tumors derived from 4 independent NPC cultures were independently sorted for DsRed expressionwith FACSAria II and directly harvested in Trizol (Invitrogen) containing tubes.. At least 0.1 µg RNA was send to BGI genomics (BGI, Shenzhen, China) and sequenced on BGISEQ-500 RS generating 50 base-pair single-end reads. Raw data from "Glia, Neurons, and Vascular Cells of the Cerebral Cortex transcriptome database" were obtained from literature (GSE52564; [24]) as fastq files and analyzed in parallel with our data. The high-quality clean tags were mapped to reference genome (mm10) using STAR [25]. To quantify the gene expression level, RSEM analysis was carried out [26], acquiring expected read counts of each gene for each sample, based on the mapping results. These data were used for successive analyses. Normalization, data trimming and differential expression analysis were performed by edgeR [27]. Principal component analysis (PCA) and heatmap representations are based on the 5% most differentially expressed gene between

neuroepithelial-derived lineages (astrocytes, neurons, mature and immature oligodendrocytes and OPCs). GoTerm enrichment analysis was carried with ClueGO [28] plugin for Cytoscape [29].

Raw and processed data are available on GEO Dataset (Accession number GSE109614).

3. Results

3.1. Mice transplanted with $_{mHGG}$PDGF and $_{mHGG}$EGFRvIII tumor cells developed high-grade gliomas.

Murine gliomas driven by the overexpression of PDGF-B (herein referred as to $_{mHGG}$PDGF) were generated by transplanting adult BALB/c mouse brains with murine NPC explanted at embryonic day 14 (E14) and transduced with a PDGF-B overexpressing retroviral vector as previously described (Fig. 1A, [30]). All mice injected (n=16, from 5 independent embryonic NPC cultures, herein after referred as to PDGF-group) developed neurological symptoms due to gliomas between 24 and 169 days after transplant (Fig. 1B).. On the contrary of PDGF-B transduction, EGFRvIII transduction is not able, by alone, to drive glioma formation from wild type NPCs and needs further alterations, such as the disruption of INK4a locus [31, 32]. Therefore, to develop a second model of glioma, based on EGFRvIII overexpression, we employed E14 NPC derived from INK4a knock-out mice [12]. In order to assess whether the disruption of INK4a locus would alter the identity of NPC population or their differentiation potential we compared the expression of cell-lineage marker between telecephalic cells derived from E14 wild-type and INK4a$^{-/-}$ embryos 2 hours after tissue dissociation and plating. The analysis revealed no gross changes in the percentage of nestin-positive progenitor cells (nExp=5, Fig. 1B), nor in the percentage of cells expressing the radial/astroglial marker GLAST and the oligodendrocyte progenitor cells markers Olig2 and PDGFRα (Fig. 1B). Analogously, no difference was observed in the differentiation ability of INK4a$^{-/-}$ NPC in term of expression of neural cell lineage markers (Fig 1C-D) after 7 days in differentiation medium. All these experiments, indicate that homozygous deletion of the INK4a locus doesn't grossly alter the identity and the fate of NPC.

Four independent E14 INK4a$^{-/-}$ NPC cultures were transduced with the vector carrying EGFR-vIII and DsRed. Cells were then orthotopically transplanted in 20 adult wild-type BALB/c mice (herein after referred

as to EGFRvIII –group, Fig. 1A). All the mice injected but two developed neurological symptoms between 27 and 141 days after transplant as a consequence of developing a glioma (Fig. 1E).

All transplanted mice were killed as soon as they showed neurological symptoms. Brains of both PDGF- and EGFRvIII-groups showed large DsRed positive tumor masses (Fig 1G,H). Cell derived from microdissection of tumor masses from both groups were maintained in culture in a serum-free medium optimized for the growth of neural stem cells. Primary tumor cells were tested to generate secondary tumors after up to 15 passages in culture. Cells derived from three independent tumors induced by PDGF-B ($_{mHGG}$PDGF) and six independent tumors induced by EGFRvIII ($_{mHGG}$EGFRvIII) were transplanted in adult BALB/c mice. All the mice transplanted with cells derived from $_{mHGG}$PDGF tumors showed neurological symptoms within 39 days (n=17) and DsRed-positive masses were observed in all their brains. Among the mice transplanted with $_{mHGG}$EGFRvIII (n=56), only 37 developed neurological symptoms within 77 days (Fig. 1F) and showed large DsRed-positive tumor masses (Fig. I,J). The remaining mice (n=19) were killed within 155 days after transplant and were found devoid of Ds-Red positive cells (data not shown). Altogether, data suggest that $_{mHGG}$EGFRvIII are less aggressive than $_{mHGG}$PDGF, at least upon secondary transplantation.

3.2. Neuropathological characterization of $_{mHGG}$PDGF and $_{mHGG}$EGFRvIII

Gliomas obtained from transplant of $_{mHGG}$PDGF or $_{mHGG}$EGFRvIII cells were analyzed in blind. Histologically, $_{mHGG}$PDGF tumors were highly cellularized and showed a strong infiltrating behavior with poorly defined tumor borders and diffusion along the white matter fibers and periventricular space (Fig. 2A,B). $_{mHGG}$PDGF were composed by mitotically active small/medium size cells with hyperchromatic nuclei and showed pseudopalisading necrotic foci as well as hypertrophic vessels, some of which were proliferating. $_{mHGG}$EGFRvIII tumors were also densely cellulated and composed by small/medium size cells, but with a more uniform size and definite oligodendroglial-like appearance, as compared to the $_{mHGG}$PDGF tumor model. (Fig. 2B). Interestingly, these tumors showed better defined borders even infiltrating single cells showed prominent neuronal satellitosis in the adjacent brain parenchyma.

Mitotic index appeared high in both models, although the proportion of cell expressing the proliferating marker Ki67 were significantly higher in $_{mHGG}$EGFRvIII (Fig. 2C,D). As expected, $_{mHGG}$EGFRvIII expressed EGFRvIII and, consequently, showed diffuse and intense EGFR expression, as assayed by both a pan-EGFR and EGFRvIII specific immunostainings. All the other markers appeared expressed with similar pattern in

both models with SOX2 and Olig2 expressed by virtually all tumor cells, high level of S100, ATRX preservation, IDH1-R132H and p53 not expressed (Fig. 2C,D). Of note, GFAP immunostaining resulted virtually negative in both models, highlighting only sparse intratumoral reactive astrocytes, in line with a proneural and oligodendroglia-like phenotype (Fig. 2C). Immunofluorescence staining demonstrated that GFAP-positive cells were bystander astrocytes rather than cancer cells since they did not express the retroviral driven reporter DsRed (Fig. 2E). Overall, although $_{mHGG}$PDGF showed a more aggressive and infiltrating phenotype, the two models appeared unexpectedly histologically similar, both sharing proneural oligodendrocyte-like features, despite difference in the underlying molecular alteration.

3.3. Molecular profiling of cultured mHGGPDGF and mHGGEGFRvIII cells revealed close similarities

In order to substantiate similarity of the two models, as suggested by pathological analysis, gene-expression profiling was performed by microarray starting from biological replicates of cells grown *in vitro*, derived from primary $_{mHGG}$PDGF (n=2) or $_{mHGG}$EGFRvIII (n=4) different tumors (Fig. 3A). Unsupervised hierarchical clustering based on Euclidean distances extended to all genes, grouped the two type of tumors in two distinct cluster (Fig. 3B). However, differential expression analysis revealed a strong similarity between the two groups. The gene annotation enrichment analysis based on BP-GOTERM associated to 50 most differentially expressed genes (DEGs) failed to identify any meaningful gene cluster. $_{mHGG}$EGFRvIII appeared slightly more differentiated showing higher expression of macroglial lineage markers (GFAP, MBP, s100), although to levels much lower than in the respective cell types.

In order to characterize the cell phenotype of $_{mHGG}$PDGF and $_{mHGG}$EGFRvIII gliomas, we compared their transcription profiles with those obtained with the same microarray platform by other groups from: murine astrocytes, neurons, oligodendrocyte progenitor cells and mature oligodendrocytes [18]; sub-ventricular zone stem cells (SVZ [19]); olfactory bulb stem cells (OBSC [20]); radial glia cells from E18 mouse embryo [21].

Results were summarized by a principal component analysis (PCA; Fig. 3D), based on the subset of most differently expressed genes between the wild type lineages. In the PCA, $_{mHGG}$PDGF and $_{mHGG}$EGFRvIII tumor cells appeared in between OPCs and SVZ cells, closest to the first.

Unsupervised hierarchical gene clustering of all the samples confirmed that both $_{mHGG}$PDGF and $_{mHGG}$EGFRvIII tumor cells clustered together with OPCs. Interestingly, OPCs expression profile was more correlated to that of mHGG cells than to the profile of adult neural stem cells.

3.4. RNA-seq analysis from ex-vivo samples confirmed that both models clusterize with OPCs.

Since murine tumor cells underwent to some passages in culture before being collected for genome-expression analyses, we asked whether the high similarity found between $_{mHGG}$PDGF and $_{mHGG}$EGFRvIII tumor expression profiles was due to biases related to culture conditions rather than reflecting the real composition of tumor transcriptomes.

We therefore analyzed acutely dissociated cells from $_{mHGG}$PDGF and $_{mHGG}$EGFRvIII tumor masses derived from the injection of 4 independent NPC cultures, isolated by fluorescence-activated cell sorting (FACS), based on the expression of the fluorescent reporter DsRed. RNA extracted from purified cell populations was sequenced on the BGISEQ-500 RS platform, obtaining 41.3±3.7 million 50bp reads per sample.

An unsupervised hierarchical clustering of transcriptome profiles taking account of all genes showed that the samples grouped in two different clusters according to the molecular lesion that induced them analogously to what observed in microarray data (data not shown). The analysis showed that the majority of DEGs were overexpressed in $_{mHGG}$PDGF (Fig. 4A). Moreover, gene annotation enrichment analysis on BP-GOTERM revealed that while the set of DEGs overexpressed by $_{mHGG}$EGFRvIII did not make a coherent picture, the set of DEGs overexpressed by $_{mHGG}$PDGF was clearly enriched in genes whose function is connected with the regulation of immune system (Fig 4B).

The transcriptome profiles of freshly dissociated $_{mHGG}$PDGF and $_{mHGG}$EGFRvIII cells were then compared to those of the main lineages of murine CNS (astrocytes, neurons, OPCs, oligodendrocytes and microglia) derived from publicly available repository [24]. The PCA analysis and the unsupervised hierarchical clustering based on the most differentially expressed genes between neuroepitalial derived lineages confirmed that $_{mHGG}$PDGF and $_{mHGG}$EGFRvIII cluster together and their closest group among the healthy neural phenotypes is represented by the OPCs (Fig. 4C,D). In the reported PCA analysis microglial cell profiles were omitted since they appeared so different from all the other cell types to dominate the first component of the PCA, compressing the differences between the other lineages on the second and further components, thereby hampering their separation.

In addition, in order to assign $_{mHGG}$PDGF and $_{mHGG}$EGFRvIII to a glioma molecular subclass, we used Classification to Nearest Centroids' (ClaNC) algorithm [33] to build a model classifier using as training set data derived from The Cancer Genome Atlas (TCGA Research Network: http://cancergenome.nih.gov/), as described in the materials and methods section. We then used the classifier generated to allocate mHGGPDGF and mHGGEGFRvIII to their molecular subclass basing on their expression profile (Fig. 4E). This analysis showed that the profile of both $_{mHGG}$PDGF and $_{mHGG}$EGFRvIII are compatible with the proneural class, corroborating the picture emerged from the histopathological analysis.

3.5. EGFRvIII expression induces NPC to acquire an oligodendroglial identity

We previously demonstrated that the bias toward the oligodendroglial lineage observed in E14 NPC transduced with PDGF-B is due to a "de novo" induction of OPC phenotype rather than to a selective proliferation of already committed precursors [10]. We asked if a similar effect is responsible of the bias towards the OPC lineages of mHGGEGFRvIII gliomas, and we therefore carried the same clonal analysis as previously done for PDGF-B (Fig. 5A). NPC from INK4a-/- E14 embryos were transduced with low titre EGFRvIII-expressing or control virus, both carrying EGFP as reporter genes. After 7 days cultures were fixed and immunostained. Clonal progeny of each transduced progenitor was identified basing on the spatial clustering of EGFP expressing cells (Fig. 1 A). The analysis showed that OPC, defined basing on Ng2 expression, were three times more frequent in EGFRvIII transduced cells than in the control (38±7% vs 13±4%, t-test $p<0.01$ Fig. 5B). This increase in Ng2-positive cells was paralleled with a similar increase in the percentage of clones containing at least one Ng2-positive cell (Ng2-clones; from 38±8% to 11±3%, $p<0.01$; Fig. 5C). On the contrary, neither the prevalence of Ng2-positive cells inside the Ng2-clones (Fig. 5D) nor their size (Fig. 5E), were different. These results are consistent with a scenario were EGFRvIII overexpression, similarly to PDGF-B, drives multipotent progenitor cells towards an OPC fate rather than to selectively increase proliferation of already committed OPC cells. In the latter case, the frequency of Ng2-clones is expected to be unchanged while Ng2 prevalence in clones and Ng2-clone size should be increased.

4. Discussion

Glioma modelling is essential in order to develop novel therapies. Syngeneic immunocompetent models are particularly interesting when focusing on the interaction between therapy and immune system [34-37]. One of the common way to create syngeneic glioma models relies on the reproduction of genetic alterations

known to be involved in the formation of human gliomas. Since PDGF and EGF pathway alterations are respectively landmarks of the proneural and classical GBM subtypes in human [2, 11], the introduction of such alterations was expected to generate models representative of the two GBM subtypes [38, 39]. PDGF-B has been reported to induce mainly low grade gliomas when transduced in post-natal GFAP-positive cells. However, high grade gliomas with oligodendroglial features resembling human proneural subtype are known to be induced by PDGF-B overexpression in embryonic progenitor cells [10] or by using lentiviral vectors in the dentate gyrus of adult mice [9]. EGFRvIII induced tumors in INK4a$^{-/-}$ mouse background have been described to generate tumor resembling high-grade astrocytomas [40, 41]. Former studies, however, reported that the expression of EGFRvIII in a subset of glial cells in the same mouse background give rise to gliomas with oligodendroglial features [42], similar to those induced by PDGF-B. These contrasting observations could be due to the use of different cells of origin that is known to contribute to tumor subtype acquisition [43-45] and could mask or alter the effective potentiality of the driver mutation. We therefore decided to unbiasedly clarify the role of the driver mutation via a direct comparison between the glioma models induced by them. We thus introduced the molecular alterations in NPC at early stages of neurogenesis that have the ability to give rise to all the neuroepithelial lineages of the central nervous system (CNS) [46]. In our opinion, this represents the best benchmark to challenge the notion that given molecular subtypes depend on specific driver mutations. We, for the first time, performed a thorough comparison between the EGFRvIII and PDGF-B induced gliomas encompassing an accurate histopathological description and transcriptomic analysis carried out by both microarrays and RNA-seq. In order to interpret our transcriptomic data, we made an effort to frame them in the context of expression profiles of all the CNS neuroepithelial lineages. Overall, our data showed that the two models are indeed very similar, sharing a proneural and oligodendroglioma-like traits and differing only on marginal aspects, suggesting that, even when occurring in unrestricted progenitor cells, the driver mutation is not necessarily predictive of the tumor phenotype in animal models. The molecular analysis confirmed this view, revealing that cells composing both $_{mHGG}$PDGF and $_{mHGG}$EGFRvIII share an OPC-like phenotype. The principal component analysis based on the expression levels of the genes with higher variance among the main lineages of CNS, shows that both models consistently ended almost equidistant from neurons, astroglia and mature oligodendrocytes. Among the progenitor cells represented in the picture (late foetal radial glia, adult SVZ neural stem, and OPCs),

$_{mHGG}$PDGF and $_{mHGG}$EGFRvIII resulted closest to OPCs/NG2-Glia, which represents the largest dividing population in the murine adult brain [47].

The main difference in molecular profiles of $_{mHGG}$PDGF and $_{mHGG}$EGFRvIII are related to genes involved in the immune-response regulation. This could represent a first hint of the existence of a deeper difference between $_{mHGG}$PDGF and $_{mHGG}$EGFRvIII at the level of microenvironment that could be underestimated by the analysis of the phenotype of the sole tumor cells. Transcriptomic data are in line with previous studies showing the existence of a mutual reshape between tumor and immune cells [48-50] and suggest that the immune microenvironment influences and contributes to the overall heterogeneity shown in glioma subtypes. Interestingly, the acquisition of a marked immune-evasive phenotype has been recently described in the progression from low- to high-grade gliomas in a related PDGF-B induced gliomas [51] and is correlated to high malignancy and to a reshape of the immune tumor microenvironment. Indeed, $_{mHGG}$PDGF showed a higher penetrance compared to $_{mHGG}$EGFRvIII, which is able to successfully root in only 70% of transplanted mice (versus 100% in $_{mHGG}$PDGF) and suggested that the immune-evasive phenotype could be induced, at least in part, by PDGF-B overexpression rather than representing a mandatory step in all glioma progression. Further analyses specifically focused on tumor-associated cells are however necessary to clarify the role of tumor microenvironment on glioma heterogeneity.

5. Acknowledgments

This work was supported by European Research Council (ERC) advanced grant number 340060 to PM; by Compagnia di San Paolo, Turin, Italy (grant no 2015.9834) "Terapie innovative per il glioblastoma" to PM; by The Italian Ministry of Health (5x1000 2014, 2015,2016).

6. Funding

This work was supported by European Research Council (ERC) advanced grant number 340060 to PM; by Compagnia di San Paolo, Turin, Italy (grant no 2015.9834) "Terapie innovative per il glioblastoma" to PM; by The Italian Ministry of Health (5x1000 2014,2015,2016).

7. Conflicts of interest

The authors declare they have no conflicts of interest.

8. References

[1] C.W. Brennan, R.G. Verhaak, A. McKenna, B. Campos, H. Noushmehr, S.R. Salama, S. Zheng, D. Chakravarty, J.Z. Sanborn, S.H. Berman, R. Beroukhim, B. Bernard, C.J. Wu, G. Genovese, I. Shmulevich, J. Barnholtz-Sloan, L. Zou, R. Vegesna, S.A. Shukla, G. Ciriello, W.K. Yung, W. Zhang, C. Sougnez, T. Mikkelsen, K. Aldape, D.D. Bigner, E.G. Van Meir, M. Prados, A. Sloan, K.L. Black, J. Eschbacher, G. Finocchiaro, W. Friedman, D.W. Andrews, A. Guha, M. Iacocca, B.P. O'Neill, G. Foltz, J. Myers, D.J. Weisenberger, R. Penny, R. Kucherlapati, C.M. Perou, D.N. Hayes, R. Gibbs, M. Marra, G.B. Mills, E. Lander, P. Spellman, R. Wilson, C. Sander, J. Weinstein, M. Meyerson, S. Gabriel, P.W. Laird, D. Haussler, G. Getz, L. Chin, The somatic genomic landscape of glioblastoma, Cell, 155 (2013) 462-477.

[2] R.G. Verhaak, K.A. Hoadley, E. Purdom, V. Wang, Y. Qi, M.D. Wilkerson, C.R. Miller, L. Ding, T. Golub, J.P. Mesirov, G. Alexe, M. Lawrence, M. O'Kelly, P. Tamayo, B.A. Weir, S. Gabriel, W. Winckler, S. Gupta, L. Jakkula, H.S. Feiler, J.G. Hodgson, C.D. James, J.N. Sarkaria, C. Brennan, A. Kahn, P.T. Spellman, R.K. Wilson, T.P. Speed, J.W. Gray, M. Meyerson, G. Getz, C.M. Perou, D.N. Hayes, Integrated genomic analysis identifies clinically relevant subtypes of glioblastoma characterized by abnormalities in PDGFRA, IDH1, EGFR, and NF1, Cancer Cell, 17 (2010) 98-110.

[3] F. De Bacco, A. D'Ambrosio, E. Casanova, F. Orzan, R. Neggia, R. Albano, F. Verginelli, M. Cominelli, P.L. Poliani, P. Luraghi, G. Reato, S. Pellegatta, G. Finocchiaro, T. Perera, E. Garibaldi, P. Gabriele, P.M. Comoglio, C. Boccaccio, MET inhibition overcomes radiation resistance of glioblastoma stem-like cells, EMBO Mol Med, 8 (2016) 550-568.

[4] M. Cominelli, S. Grisanti, S. Mazzoleni, C. Branca, L. Buttolo, D. Furlan, B. Liserre, M.F. Bonetti, D. Medicina, V. Pellegrini, M. Buglione, R. Liserre, S. Pellegatta, G. Finocchiaro, P. Dalerba, F. Facchetti, M. Pizzi, R. Galli, P.L. Poliani, EGFR amplified and overexpressing glioblastomas and association with better response to adjuvant metronomic temozolomide, J Natl Cancer Inst, 107 (2015).

[5] K.P.L. Bhat, V. Balasubramaniyan, B. Vaillant, R. Ezhilarasan, K. Hummelink, F. Hollingsworth, K. Wani, L. Heathcock, J.D. James, L.D. Goodman, S. Conroy, L. Long, N. Lelic, S. Wang, J. Gumin, D. Raj, Y. Kodama, A. Raghunathan, A. Olar, K. Joshi, C.E. Pelloski, A. Heimberger, S.H. Kim, D.P. Cahill, G. Rao, W.F.A. Den Dunnen, H. Boddeke, H.S. Phillips, I. Nakano, F.F. Lang, H. Colman, E.P. Sulman, K. Aldape, Mesenchymal

differentiation mediated by NF-kappaB promotes radiation resistance in glioblastoma, Cancer Cell, 24 (2013) 331-346.

[6] M. Li, A. Xiao, D. Floyd, I. Olmez, J. Lee, J. Godlewski, A. Bronisz, K.P.L. Bhat, E.P. Sulman, I. Nakano, B. Purow, CDK4/6 inhibition is more active against the glioblastoma proneural subtype, Oncotarget, 8 (2017) 55319-55331.

[7] I. Crespo, A.L. Vital, M. Gonzalez-Tablas, C. Patino Mdel, A. Otero, M.C. Lopes, C. de Oliveira, P. Domingues, A. Orfao, M.D. Tabernero, Molecular and Genomic Alterations in Glioblastoma Multiforme, Am J Pathol, 185 (2015) 1820-1833.

[8] C. Dai, J.C. Celestino, Y. Okada, D.N. Louis, G.N. Fuller, E.C. Holland, PDGF autocrine stimulation dedifferentiates cultured astrocytes and induces oligodendrogliomas and oligoastrocytomas from neural progenitors and astrocytes in vivo, Genes Dev, 15 (2001) 1913-1925.

[9] G.J. Rahme, B.W. Luikart, C. Cheng, M.A. Israel, A recombinant lentiviral PDGF-driven mouse model of proneural glioblastoma, Neuro Oncol, 20 (2018) 332-342.

[10] I. Appolloni, F. Calzolari, E. Tutucci, S. Caviglia, M. Terrile, G. Corte, P. Malatesta, PDGF-B induces a homogeneous class of oligodendrogliomas from embryonic neural progenitors, Int J Cancer, 124 (2009) 2251-2259.

[11] C. Brennan, H. Momota, D. Hambardzumyan, T. Ozawa, A. Tandon, A. Pedraza, E. Holland, Glioblastoma subclasses can be defined by activity among signal transduction pathways and associated genomic alterations, PLoS One, 4 (2009) e7752.

[12] M. Serrano, H. Lee, L. Chin, C. Cordon-Cardo, D. Beach, R.A. DePinho, Role of the INK4a locus in tumor suppression and cell mortality, Cell, 85 (1996) 27-37.

[13] I. Appolloni, F. Calzolari, G. Corte, R. Perris, P. Malatesta, Six3 controls the neural progenitor status in the murine CNS, Cereb Cortex, 18 (2008) 553-562.

[14] I. Appolloni, M. Barilari, S. Caviglia, E. Gambini, E. Reisoli, P. Malatesta, A cadherin switch underlies malignancy in high-grade gliomas, Oncogene, 34 (2015) 1991-2002.

[15] M. Terrile, I. Appolloni, F. Calzolari, R. Perris, E. Tutucci, P. Malatesta, PDGF-B-driven gliomagenesis can occur in the absence of the proteoglycan NG2, BMC Cancer, 10 (2010) 550.

[16] I. Appolloni, F. Calzolari, M. Barilari, M. Terrile, A. Daga, P. Malatesta, Antagonistic modulation of gliomagenesis by Pax6 and Olig2 in PDGF-induced oligodendroglioma, International journal of cancer. Journal international du cancer, 131 (2012) E1078-1087.

[17] J.E. Bottenstein, G.H. Sato, Growth of a rat neuroblastoma cell line in serum-free supplemented medium, Proc Natl Acad Sci U S A, 76 (1979) 514-517.

[18] J.D. Cahoy, B. Emery, A. Kaushal, L.C. Foo, J.L. Zamanian, K.S. Christopherson, Y. Xing, J.L. Lubischer, P.A. Krieg, S.A. Krupenko, W.J. Thompson, B.A. Barres, A transcriptome database for astrocytes, neurons, and oligodendrocytes: a new resource for understanding brain development and function, J Neurosci, 28 (2008) 264-278.

[19] Y.H. Chen, L.D. McGowan, P.J. Cimino, S. Dahiya, J.R. Leonard, D.Y. Lee, D.H. Gutmann, Mouse low-grade gliomas contain cancer stem cells with unique molecular and functional properties, Cell Rep, 10 (2015) 1899-1912.

[20] V. Nieto-Estevez, J. Pignatelli, M.J. Arauzo-Bravo, A. Hurtado-Chong, C. Vicario-Abejon, A global transcriptome analysis reveals molecular hallmarks of neural stem cell death, survival, and differentiation in response to partial FGF-2 and EGF deprivation, PLoS One, 8 (2013) e53594.

[21] L. Pinto, M.T. Mader, M. Irmler, M. Gentilini, F. Santoni, D. Drechsel, R. Blum, R. Stahl, A. Bulfone, P. Malatesta, J. Beckers, M. Gotz, Prospective isolation of functionally distinct radial glial subtypes--lineage and transcriptome analysis, Mol Cell Neurosci, 38 (2008) 15-42.

[22] R Core Team, R: A language and environment for statistical computing., R Foundation for Statistical Computing, Vienna, Austria, 2017.

[23] B.M. Bolstad, R.A. Irizarry, M. Astrand, T.P. Speed, A comparison of normalization methods for high density oligonucleotide array data based on variance and bias, Bioinformatics, 19 (2003) 185-193.

[24] Y. Zhang, K. Chen, S.A. Sloan, M.L. Bennett, A.R. Scholze, S. O'Keeffe, H.P. Phatnani, P. Guarnieri, C. Caneda, N. Ruderisch, S. Deng, S.A. Liddelow, C. Zhang, R. Daneman, T. Maniatis, B.A. Barres, J.Q. Wu, An RNA-sequencing transcriptome and splicing database of glia, neurons, and vascular cells of the cerebral cortex, J Neurosci, 34 (2014) 11929-11947.

[25] A. Dobin, T.R. Gingeras, Mapping RNA-seq Reads with STAR, Curr Protoc Bioinformatics, 51 (2015) 11 14 11-19.

[26] B. Li, C.N. Dewey, RSEM: accurate transcript quantification from RNA-Seq data with or without a reference genome, BMC Bioinformatics, 12 (2011) 323.

[27] M.D. Robinson, D.J. McCarthy, G.K. Smyth, edgeR: a Bioconductor package for differential expression analysis of digital gene expression data, Bioinformatics, 26 (2010) 139-140.

[28] G. Bindea, B. Mlecnik, H. Hackl, P. Charoentong, M. Tosolini, A. Kirilovsky, W.H. Fridman, F. Pages, Z. Trajanoski, J. Galon, ClueGO: a Cytoscape plug-in to decipher functionally grouped gene ontology and pathway annotation networks, Bioinformatics, 25 (2009) 1091-1093.

[29] P. Shannon, A. Markiel, O. Ozier, N.S. Baliga, J.T. Wang, D. Ramage, N. Amin, B. Schwikowski, T. Ideker, Cytoscape: a software environment for integrated models of biomolecular interaction networks, Genome Res, 13 (2003) 2498-2504.

[30] E. Gambini, E. Reisoli, I. Appolloni, V. Gatta, G. Campadelli-Fiume, L. Menotti, P. Malatesta, Replication-competent herpes simplex virus retargeted to HER2 as therapy for high-grade glioma, Mol Ther, 20 (2012) 994-1001.

[31] E.C. Holland, W.P. Hively, R.A. DePinho, H.E. Varmus, A constitutively active epidermal growth factor receptor cooperates with disruption of G1 cell-cycle arrest pathways to induce glioma-like lesions in mice, Genes Dev, 12 (1998) 3675-3685.

[32] H. Zhu, J. Acquaviva, P. Ramachandran, A. Boskovitz, S. Woolfenden, R. Pfannl, R.T. Bronson, J.W. Chen, R. Weissleder, D.E. Housman, A. Charest, Oncogenic EGFR signaling cooperates with loss of tumor suppressor gene functions in gliomagenesis, Proc Natl Acad Sci U S A, 106 (2009) 2712-2716.

[33] A.R. Dabney, Classification of microarrays to nearest centroids, Bioinformatics, 21 (2005) 4148-4154.

[34] E. Reisoli, E. Gambini, I. Appolloni, V. Gatta, M. Barilari, L. Menotti, P. Malatesta, Efficacy of HER2 retargeted herpes simplex virus as therapy for high-grade glioma in immunocompetent mice, Cancer Gene Ther, 19 (2012) 788-795.

[35] F. Alessandrini, L. Menotti, E. Avitabile, I. Appolloni, D. Ceresa, D. Marubbi, G. Campadelli-Fiume, P. Malatesta, Eradication of glioblastoma by immuno-virotherapy with a retargeted oncolytic HSV in a preclinical model, Oncogene, 38 (2019) 4467-4479.

[36] H. Nakashima, Q.A. Alayo, P. Penaloza-MacMaster, G.J. Freeman, V.K. Kuchroo, D.A. Reardon, S. Fernandez, M. Caligiuri, E.A. Chiocca, Modeling tumor immunity of mouse glioblastoma by exhausted CD8(+) T cells, Sci Rep, 8 (2018) 208.

[37] A.T. Yeo, A. Charest, Immune Checkpoint Blockade Biology in Mouse Models of Glioblastoma, J Cell Biochem, 118 (2017) 2516-2527.

[38] L. Janbazian, J. Karamchandani, S. Das, Mouse models of glioblastoma: lessons learned and questions to be answered, J Neurooncol, 118 (2014) 1-8.

[39] Y. Shen, J. Li, M. Nitta, D. Futalan, T. Steed, J.M. Treiber, Z. Taich, D. Stevens, J. Wykosky, H.Z. Chen, B.S. Carter, O.J. Becher, R. Kennedy, F. Esashi, J.N. Sarkaria, F.B. Furnari, W.K. Cavenee, A. Desai, C.C. Chen, Orthogonal targeting of EGFRvIII expressing glioblastomas through simultaneous EGFR and PLK1 inhibition, Oncotarget, 6 (2015) 11751-11767.

[40] R.M. Bachoo, E.A. Maher, K.L. Ligon, N.E. Sharpless, S.S. Chan, M.J. You, Y. Tang, J. DeFrances, E. Stover, R. Weissleder, D.H. Rowitch, D.N. Louis, R.A. DePinho, Epidermal growth factor receptor and Ink4a/Arf: convergent mechanisms governing terminal differentiation and transformation along the neural stem cell to astrocyte axis, Cancer Cell, 1 (2002) 269-277.

[41] O.R. Lindberg, A. McKinney, J.R. Engler, G. Koshkakaryan, H. Gong, A.E. Robinson, A.J. Ewald, E. Huillard, C. David James, A.M. Molinaro, J.T. Shieh, J.J. Phillips, GBM heterogeneity as a function of variable epidermal growth factor receptor variant III activity, Oncotarget, 7 (2016) 79101-79116.

[42] W.A. Weiss, M.J. Burns, C. Hackett, K. Aldape, J.R. Hill, H. Kuriyama, N. Kuriyama, N. Milshteyn, T. Roberts, M.F. Wendland, R. DePinho, M.A. Israel, Genetic determinants of malignancy in a mouse model for oligodendroglioma, Cancer Res, 63 (2003) 1589-1595.

[43] S.R. Alcantara Llaguno, Z. Wang, D. Sun, J. Chen, J. Xu, E. Kim, K.J. Hatanpaa, J.M. Raisanen, D.K. Burns, J.E. Johnson, L.F. Parada, Adult Lineage-Restricted CNS Progenitors Specify Distinct Glioblastoma Subtypes, Cancer Cell, 28 (2015) 429-440.

[44] Y. Jiang, V.D. Marinescu, Y. Xie, M. Jarvius, N.P. Maturi, C. Haglund, S. Olofsson, N. Lindberg, T. Olofsson, C. Leijonmarck, G. Hesselager, I. Alafuzoff, M. Fryknas, R. Larsson, S. Nelander, L. Uhrbom, Glioblastoma Cell Malignancy and Drug Sensitivity Are Affected by the Cell of Origin, Cell Rep, 18 (2017) 977-990.

[45] C. Liu, J.C. Sage, M.R. Miller, R.G. Verhaak, S. Hippenmeyer, H. Vogel, O. Foreman, R.T. Bronson, A. Nishiyama, L. Luo, H. Zong, Mosaic analysis with double markers reveals tumor cell of origin in glioma, Cell, 146 (2011) 209-221.

[46] P. Malatesta, I. Appolloni, F. Calzolari, Radial glia and neural stem cells, Cell Tissue Res, 331 (2008) 165-178.

[47] M.R. Dawson, A. Polito, J.M. Levine, R. Reynolds, NG2-expressing glial progenitor cells: an abundant and widespread population of cycling cells in the adult rat CNS, Mol Cell Neurosci, 24 (2003) 476-488.

[48] G.P. Dunn, A.T. Bruce, H. Ikeda, L.J. Old, R.D. Schreiber, Cancer immunoediting: from immunosurveillance to tumor escape, Nat Immunol, 3 (2002) 991-998.

[49] L. Hui, Y. Chen, Tumor microenvironment: Sanctuary of the devil, Cancer Lett, 368 (2015) 7-13.

[50] Q. Wang, B. Hu, X. Hu, H. Kim, M. Squatrito, L. Scarpace, A.C. deCarvalho, S. Lyu, P. Li, Y. Li, F. Barthel, H.J. Cho, Y.H. Lin, N. Satani, E. Martinez-Ledesma, S. Zheng, E. Chang, C.G. Sauve, A. Olar, Z.D. Lan, G. Finocchiaro, J.J. Phillips, M.S. Berger, K.R. Gabrusiewicz, G. Wang, E. Eskilsson, J. Hu, T. Mikkelsen, R.A. DePinho, F. Muller, A.B. Heimberger, E.P. Sulman, D.H. Nam, R.G.W. Verhaak, Tumor Evolution of Glioma-Intrinsic Gene Expression Subtypes Associates with Immunological Changes in the Microenvironment, Cancer Cell, 32 (2017) 42-56 e46.

[51] I. Appolloni, F. Alessandrini, D. Ceresa, D. Marubbi, E. Gambini, D. Reverberi, F. Loiacono, P. Malatesta, Progression from low- to high-grade in a glioblastoma model reveals the pivotal role of immunoediting, Cancer Lett, 442 (2019) 213-221.

Figure legends

Fig.1 Induction of glioblastoma models by different molecular lesions.

(A) The scheme depicts how the tumor models were generated. $_{mHGG}$PDGF were induced by orthotopic transplantation of NPC from wild-type E14 embryos following the retroviral transduction of PDGF-B. $_{mHGG}$EGFRvIII were induced by orthotopic transplantation of NPC from INK4a$^{-/-}$ E14 embryos following the retroviral transduction of EGFRvIII. Tumor masses obtained can be dissociated, cultured and intracerebrally transplanted in naïve mice, giving rise to secondary tumors. (B-D) Comparison of NPC composition and their differentiative potential in wild-type and INK4a$^{-/-}$ E14 embryos. Barplots indicate the percentage of marker-positive cells (nExp=5, error bars show the standard deviation). (B) Analysis of glial progenitor markers in acutely dissociated NPC from wild-type and INK4a$^{-/-}$ E14 embryos. (C) Analysis of mature neural lineage markers in NPC from wild-type and INK4a$^{-/-}$ E14 embryos after 7 days of *in vitro* differentiation. (D) representative micrographs showing immunoreactivity for specified markers in *in vitro* differentiated NPC. (E) Survival curves of mice transplanted with NPC overexpressing PDGF-B (green line) or EGFRvIII (red line). (F) Survival curves of mice transplanted with cells derived from primary $_{mHGG}$PDGF (green line) or $_{mHGG}$EGFRvIII (red line). (G-J) Representative dorsal images of brains harboring primary $_{mHGG}$PDGF (G), primary $_{mHGG}$EGFRvIII (H), secondary $_{mHGG}$PDGF (I) and secondary $_{mHGG}$EGFRvIII (J). DsRed fluorescent reporter expressed by tumor cells were represented in green (G,I) or in red (H,J). Scale bar: 2mm.

Fig.2 Histopatological analysis of $_{mHGG}$PDGF and $_{mHGG}$EGFRvIII

(A) Coronal brain sections of mice harboring secondary $_{mHGG}$PDGF or $_{mHGG}$EGFRvIII. In blue are shown cell nuclei (Hoechst 33342), in red the DsRed fluorescent reporter expressed by tumor cells. (B) Representative micrographs of brain sections of secondary $_{mHGG}$PDGF and $_{mHGG}$EGFRvIII stained with hematoxylin and eosin. The asterisks indicate a pseudopalisade, arrows indicate neuronal satellitosis, arrowheads indicate mitotic figures. (C) Immunohistochemical staining of section of secondary $_{mHGG}$PDGF and $_{mHGG}$EGFRvIII stained with antibodies targeting indicated proteins. (D) Histograms reporting the percentage of Olig2, Sox2 and Ki67 positive cells in $_{mHGG}$PDGF and $_{mHGG}$EGFRvIII sections. (E) Immunofluorescence microphotographs of section of secondary $_{mHGG}$PDGF or $_{mHGG}$EGFRvIII stained with anti-GFAP (green) antibody. In blue are shown nuclei; in red the tumor reporter (DsRed). Scale bars: 1mm (A), 50µm (B,C,E).

Fig.3 Microarray expression profiles of cultured $_{mHGG}$PDGF and $_{mHGG}$EGFRvIII

(A) Representative micrographs of $_{mHGG}$PDGF and $_{mHGG}$EGFRvIII derived cells cultured as monolayers. Scale bar 50 µm. (B) Hierarchical clustering of four independent $_{mHGG}$EGFRvIII- and two $_{mHGG}$PDGF- cultures. (C) Principal component analysis and (D) heatmap displaying cultured astrocytes, neurons, OPCs, oligodendrocytes, radial glia, SVZ/OB stem cells, $_{mHGG}$PDGF and $_{mHGG}$EGFRvIII profiles. PCA and heatmap were based on the 1% most differentially expressed gene between neural lineages.

Fig.4 RNA-seq expression profiles of acutely dissociated $_{mHGG}$PDGF and $_{mHGG}$EGFRvIII

(A) Volcano plot displaying differential gene expression between $_{mHGG}$EGFRvIII and $_{mHGG}$PDGF. Genes significantly upregulated in $_{mHGG}$PDGF are represented in green while those upregulated in $_{mHGG}$EGFRvIII are represented in red ($p<5x10^{-4}$). (B) Network of enriched GoTerm generated by annotation enrichment analysis of the set of differentially expressed genes. (C) Principal component analyses and (D) heatmap displaying RNA-seq data from the indicated lineages of the central nervous system and from acutely dissociated $_{mHGG}$EGFRvIII and $_{mHGG}$PDGF. (E) Heatmap representing subtype signature classification of 3 independent $_{mHGG}$EGFRvIII and 3 $_{mHGG}$PDGF generated using Classification to Nearest Centroids' (ClaNC) algorithm trained on TGCA primary human glioblastoma.

Fig.5 EGFRvIII transduction drives neural progenitors to develop as OPCs

(A) Schematic representation of the possible outcomes at the clonal level of EGFRvIII overexpression in cultured neural progenitor cells. Transduction could: (a') have no effect on NG2 expression (or even repress it); (a'') induce the expression of Ng2 thus increasing the percentage Ng2-clones (i.e. clones containing at least one Ng2-positve cell); (a''') drive the selective expansion of Ng2-positive cells thus increasing the clonal size of Ng2-clones and the abundance of Ng2-positive cells in them. (B) Percentage of Ng2-positive cells among the transduced cells. (C) Percentage Ng2-clones among all clones; (D) abundance of Ng2-positive cells in Ng2-clones. (E) Size of Ng2-clones. (B-E) Error bars show the standard error of the mean. **p < 0.01 in a 2-tailed Student's t-test.

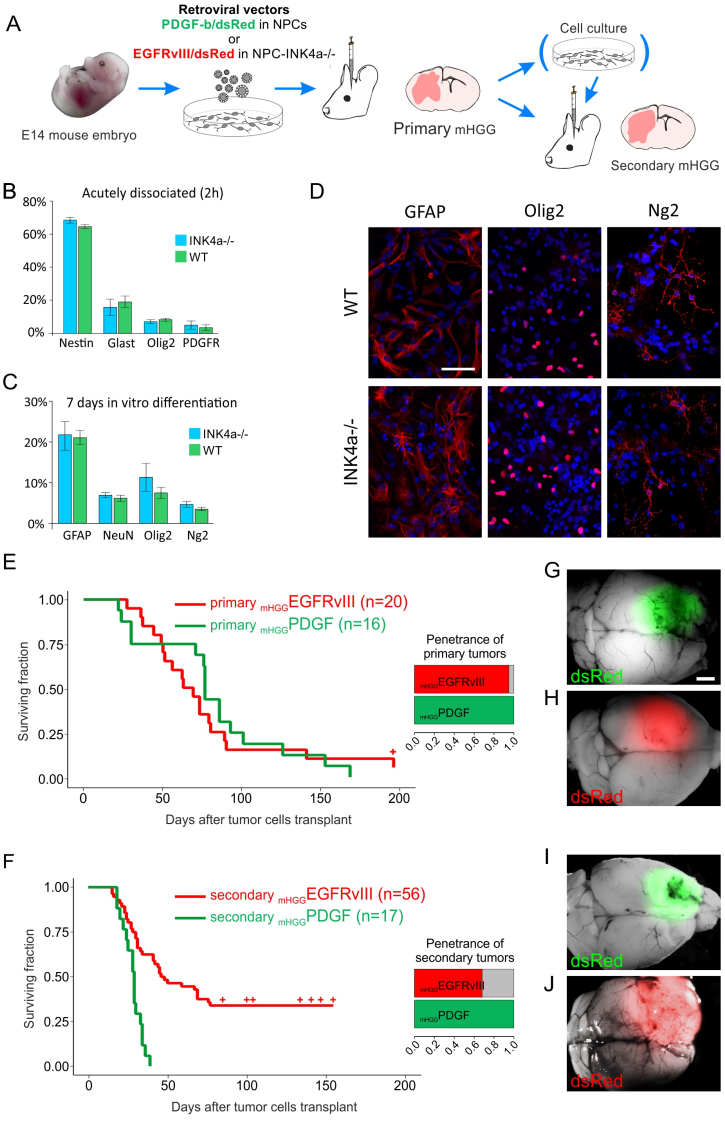
A
Retroviral vectors
PDGF-b/dsRed in NPCs
or
EGFRvIII/dsRed in NPC-INK4a-/-
E14 mouse embryo
Primary mHGG
Cell culture
Secondary mHGG
B
Acutely dissociated (2h)
INK4a-/-
WT
Nestin
Glast
Olig2
PDGFR
C
7 days in vitro differentiation
GFAP
NeuN
Olig2
Ng2
D
GFAP
Olig2
Ng2
WT
INK4a-/-
E
primary mHGGEGFRvIII (n=20)
primary mHGGPDGF (n=16)
Surviving fraction
Days after tumor cells transplant
Penetrance of primary tumors
F
secondary mHGGEGFRvIII (n=56)
secondary mHGGPDGF (n=17)
Penetrance of secondary tumors
G
H
I
J
dsRed

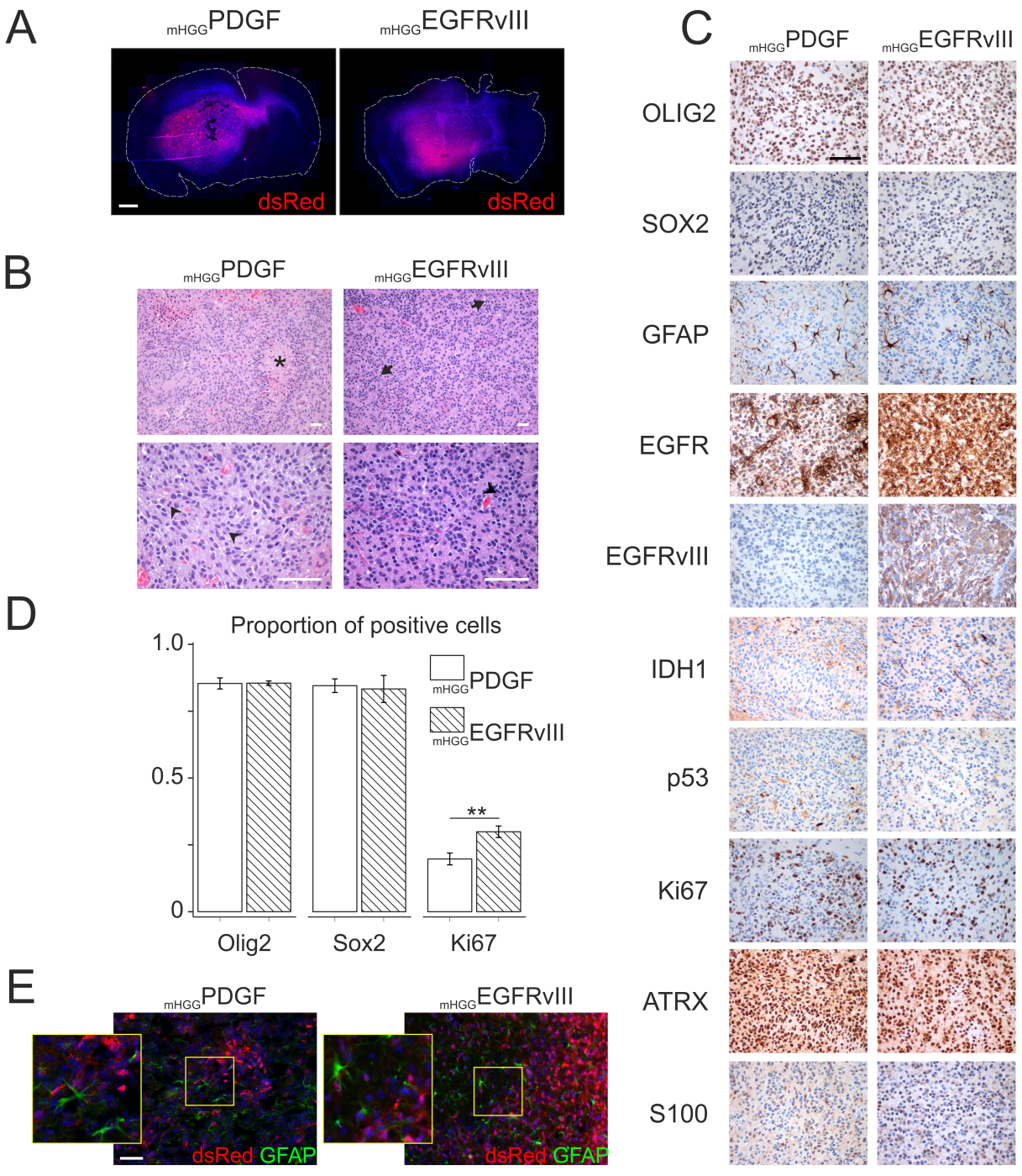
A
mHGGPDGF
mHGGEGFRvIII
dsRed
dsRed
B
mHGGPDGF
mHGGEGFRvIII
C
mHGGPDGF
mHGGEGFRvIII
OLIG2
SOX2
GFAP
EGFR
EGFRvIII
IDH1
p53
Ki67
ATRX
S100
D
Proportion of positive cells
1.0
0.5
0
mHGGPDGF
mHGGEGFRvIII
**
Olig2
Sox2
Ki67
E
mHGGPDGF
mHGGEGFRvIII
dsRed GFAP
dsRed GFAP

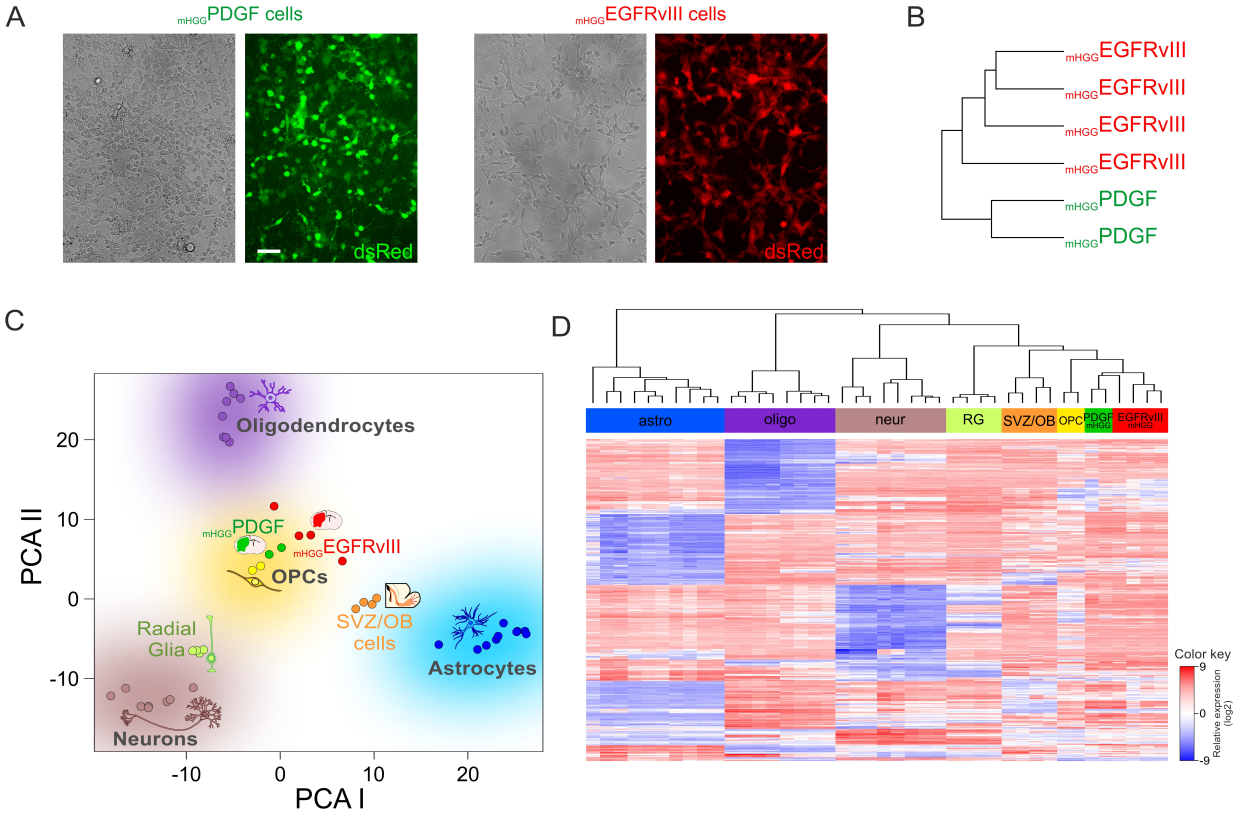
A
mHGGPDGF cells
mHGGEGFRvIII cells
dsRed
dsRed
B
mHGGEGFRvIII
mHGGEGFRvIII
mHGGEGFRvIII
mHGGEGFRvIII
mHGGPDGF
mHGGPDGF
C
Oligodendrocytes
mHGGPDGF
mHGGEGFRvIII
OPCs
SVZ/OB cells
Radial Glia
Astrocytes
Neurons
PCA II
PCA I
20
10
0
-10
-10
0
10
20
D
astro
oligo
neur
RG
SVZ/OB
OPC
PDGF mHGG
EGFRvIII mHGG
Color key
9
0
-9
Relative expression (log2)

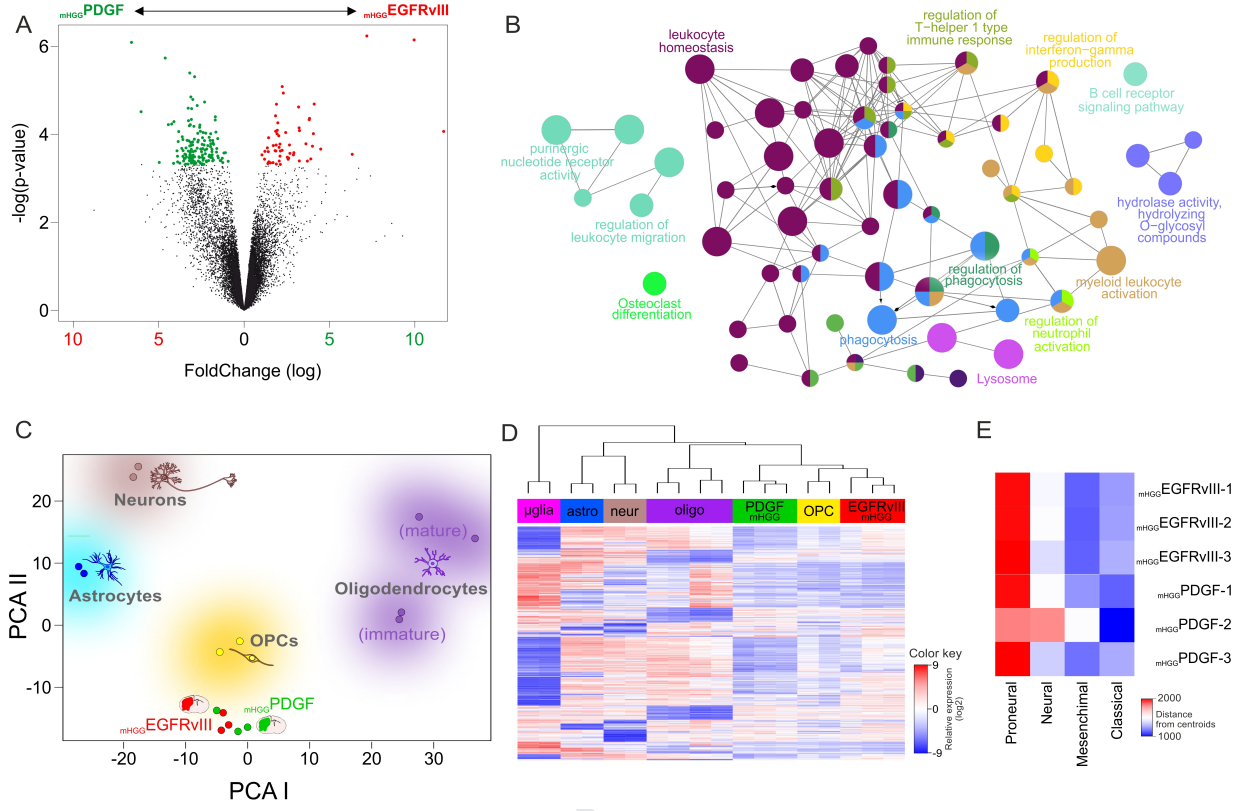
A
mHGGPDGF
mHGGEGFRvIII
-log(p-value)
FoldChange (log)
B
leukocyte homeostasis
regulation of T−helper 1 type immune response
regulation of interferon−gamma production
B cell receptor signaling pathway
purinergic nucleotide receptor activity
regulation of leukocyte migration
Osteoclast differentiation
hydrolase activity, hydrolyzing O−glycosyl compounds
regulation of phagocytosis
myeloid leukocyte activation
phagocytosis
regulation of neutrophil activation
Lysosome
C
Neurons
(mature)
Astrocytes
Oligodendrocytes
(immature)
OPCs
mHGGPDGF
mHGGEGFRvIII
PCA II
PCA I
D
μglia
astro
neur
oligo
PDGF mHGG
OPC
EGFRvIII mHGG
Color key
Relative expression (log)
E
mHGGEGFRvIII-1
mHGGEGFRvIII-2
mHGGEGFRvIII-3
mHGGPDGF-1
mHGGPDGF-2
mHGGPDGF-3
Proneural
Neural
Mesenchimal
Classical
Distance from centroids

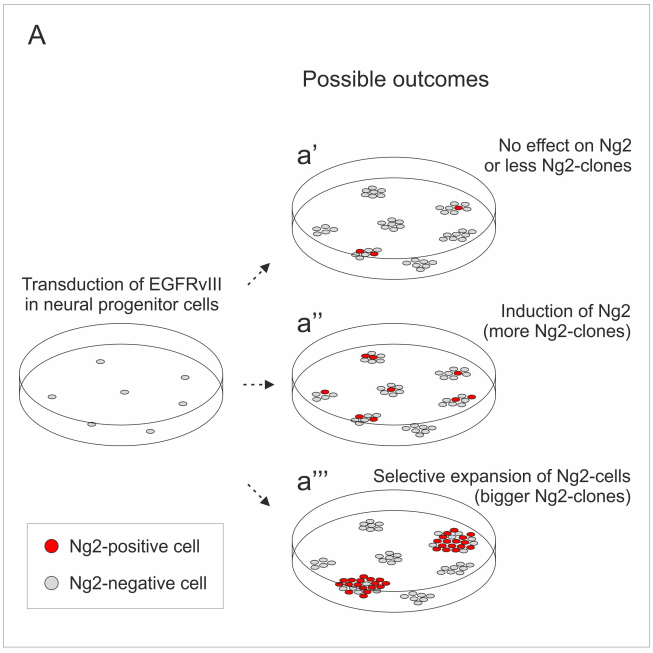

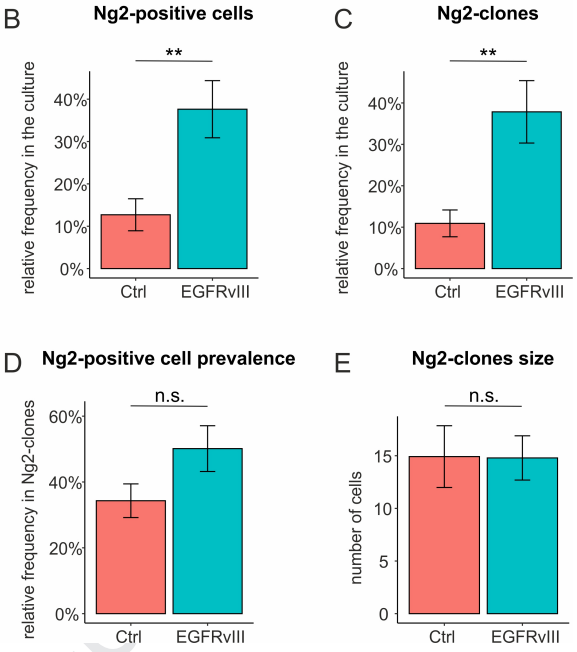

Figure legends

Fig.1 Induction of glioblastoma models by different molecular lesions.

(A) The scheme depicts how the tumor models were generated. $_{mHGG}$PDGF were induced by orthotopic transplantation of NPC from wild-type E14 embryos following the retroviral transduction of PDGF-B. $_{mHGG}$EGFRvIII were induced by orthotopic transplantation of NPC from INK4a$^{-/-}$ E14 embryos following the retroviral transduction of EGFRvIII. Tumor masses obtained can be dissociated, cultured and intracerebrally transplanted in naïve mice, giving rise to secondary tumors. (B-D) Comparison of NPC composition and their differentiative potential in wild-type and INK4a$^{-/-}$ E14 embryos. Barplots indicate the percentage of marker-positive cells (nExp=5, error bars show the standard deviation). (B) Analysis of glial progenitor markers in acutely dissociated NPC from wild-type and INK4a$^{-/-}$ E14 embryos. (C) Analysis of mature neural lineage markers in NPC from wild-type and INK4a$^{-/-}$ E14 embryos after 7 days of *in vitro* differentiation. (D) representative micrographs showing immunoreactivity for specified markers in *in vitro* differentiated NPC. (E) Survival curves of mice transplanted with NPC overexpressing PDGF-B (green line) or EGFRvIII (red line). (F) Survival curves of mice transplanted with cells derived from primary $_{mHGG}$PDGF (green line) or $_{mHGG}$EGFRvIII (red line). (G-J) Representative dorsal images of brains harboring primary $_{mHGG}$PDGF (G), primary $_{mHGG}$EGFRvIII (H), secondary $_{mHGG}$PDGF (I) and secondary $_{mHGG}$EGFRvIII (J). DsRed fluorescent reporter expressed by tumor cells were represented in green (G,I) or in red (H,J). Scale bar: 2mm.

Fig.2 Histopatological analysis of $_{mHGG}$PDGF and $_{mHGG}$EGFRvIII

(A) Coronal brain sections of mice harboring secondary $_{mHGG}$PDGF or $_{mHGG}$EGFRvIII. In blue are shown cell nuclei (Hoechst 33342), in red the DsRed fluorescent reporter expressed by tumor cells. (B) Representative micrographs of brain sections of secondary $_{mHGG}$PDGF and $_{mHGG}$EGFRvIII stained with hematoxylin and eosin. The asterisks indicate a pseudopalisade, arrows indicate neuronal satellitosis, arrowheads indicate mitotic figures. (C) Immunohistochemical staining of section of secondary $_{mHGG}$PDGF and $_{mHGG}$EGFRvIII stained with antibodies targeting indicated proteins. (D) Histograms reporting the percentage of Olig2, Sox2 and Ki67 positive cells in $_{mHGG}$PDGF and $_{mHGG}$EGFRvIII sections. (E) Immunofluorescence microphotographs of section of secondary $_{mHGG}$PDGF or $_{mHGG}$EGFRvIII stained with anti-GFAP (green) antibody. In blue are shown nuclei; in red the tumor reporter (DsRed). Scale bars: 1mm (A), 50µm (B,C,E).

Fig.3 Microarray expression profiles of cultured $_{mHGG}$PDGF and $_{mHGG}$EGFRvIII

(A) Representative micrographs of $_{mHGG}$PDGF and $_{mHGG}$EGFRvIII derived cells cultured as monolayers. Scale bar 50 µm. (B) Hierarchical clustering of four independent $_{mHGG}$EGFRvIII- and two $_{mHGG}$PDGF- cultures. (C) Principal component analysis and (D) heatmap displaying cultured astrocytes, neurons, OPCs, oligodendrocytes, radial glia, SVZ/OB stem cells, $_{mHGG}$PDGF and $_{mHGG}$EGFRvIII profiles. PCA and heatmap were based on the 1% most differentially expressed gene between neural lineages.

Fig.4 RNA-seq expression profiles of acutely dissociated $_{mHGG}$PDGF and $_{mHGG}$EGFRvIII

(A) Volcano plot displaying differential gene expression between $_{mHGG}$EGFRvIII and $_{mHGG}$PDGF. Genes significantly upregulated in $_{mHGG}$PDGF are represented in green while those upregulated in $_{mHGG}$EGFRvIII are represented in red ($p<5x10^{-4}$). (B) Network of enriched GoTerm generated by annotation enrichment analysis of the set of differentially expressed genes. (C) Principal component analyses and (D) heatmap displaying RNA-seq data from the indicated lineages of the central nervous system and from acutely dissociated $_{mHGG}$EGFRvIII and $_{mHGG}$PDGF. (E) Heatmap representing subtype signature classification of 3 independent $_{mHGG}$EGFRvIII and 3 $_{mHGG}$PDGF generated using Classification to Nearest Centroids' (ClaNC) algorithm trained on TGCA primary human glioblastoma.

Fig.5 EGFRvIII transduction drives neural progenitors to develop as OPCs

(A) Schematic representation of the possible outcomes at the clonal level of EGFRvIII overexpression in cultured neural progenitor cells. Transduction could: (a') have no effect on NG2 expression (or even repress it); (a'') induce the expression of Ng2 thus increasing the percentage Ng2-clones (i.e. clones containing at least one Ng2-positve cell); (a''') drive the selective expansion of Ng2-positive cells thus increasing the clonal size of Ng2-clones and the abundance of Ng2-positive cells in them. (B) Percentage of Ng2-positive cells among the transduced cells. (C) Percentage Ng2-clones among all clones; (D) abundance of Ng2-positive cells in Ng2-clones. (E) Size of Ng2-clones. (B-E) Error bars show the standard error of the mean. **p < 0.01 in a 2-tailed Student's t-test.

- Alteration of either PDGF or EGFR pathway induces unexpectedly similar gliomas
- Both PDGFB and EGFRvIII induced gliomas share proneural features
- Caution is needed inferring glioma subtype from driver mutations in animal models

Conflicts of interest

The authors declare they have no conflicts of interest.

Francesco Alessandrini: conceptualization, data curation, formal analysis, visualization, investigation, original draft.

Davide Ceresa: conceptualization, data curation, formal analysis, visualization, investigation, original draft, review & editing.

Irene Appolloni: conceptualization, data curation, formal analysis, investigation, original draft, review & editing.

Francesca Pagani: data curation, investigation.

Pietro Luigi Poliani: conceptualization, formal analysis, investigation.

Daniela Marubbi: data curation, investigation.

Paolo Malatesta: conceptualization, formal analysis, project administration, funding acquisition visualization, supervision, original draft, review & editing.